Synthesis, Characterization, and Molecular Structure of Cross-Linkable Rigid-Rod Liquid Crystalline Polyesters Containing Side Allyl Groups.

Domenico Acierno,[†] Eugenio Amendola,[‡] Simona Concilio,[§] Rosa Fresa,[§] Pio Iannelli,*[,§] and Paolo Vacca[§]

Dipartimento di Ingegneria dei Materiali e della Produzione, Università di Napoli, P.le Tecchio, I-80125 Napoli, Italy; Istituto per la Tecnologia dei Materiali Compositi-CNR, P.le Tecchio, I-80125 Napoli, Italy; and Dipartimento di Ingegneria Chimica ed Alimentare, Università di Salerno, via Ponte Don Melillo, I-84084 Fisciano (Salerno), Italy

Received May 15, 2000; Revised Manuscript Received September 20, 2000

ABSTRACT: The synthesis and characterization of a new class of rigid-rod liquid crystalline polyesters [**R(*n*)**] bearing side groups is reported. **R(*n*)** were prepared by interfacial polycondensation of *n*-alkoxyterephthaloyl chloride and 3,3′-diallyl-4,4′-dihydoxybiphenol exploiting the good solubility in chloroform promoted by the side flexible groups. **R(*n*)** show a mesophase at room temperature, and crystallize in some cases ($n = 4-7$) upon annealing. The crystalline phase has been resolved and refined (space group $P2_1$, 2 chains per unit cell). The molecular packing is characterized by a layered organization of chains, with pendant groups placed between layers. At high temperature, **R(*n*)** show the nematic phase. Polymers can be processed to form fibers, with the exception of **R(1)** which cross-links very quickly in the molten state. Heating at temperature over 200 °C or annealing in the solid-state induces cross-linking of allyl groups. In the latter case, the macro-orientation of fibrous samples can be quenched. **R(5)** and **R(10)** each show a constant tensile modulus of 1 and 0.5 GPa, respectively, in the range of temperature from about 150 to 300 °C.

Introduction

Rigid-rod liquid crystalline polymers (RLCPs) have been extensively investigated.[1,2] Taking advantage of the liquid crystalline (LC) behavior and the intrinsic chain stiffness, RLCPs may be processed to give fibrous samples with a very high degree of orientation and, consequently, showing outstanding mechanical performances. The main flaw of these polymers is the high melting or softening temperatures (frequently thermal decomposition occurs before this) which makes their processing difficult and sometimes impossible. Copolymerization of appropriate monomers has been extensively used to reduce melting or softening temperature. Another approach is to attach side groups to the chain backbone thus disrupting the crystalline order.[3−17] In some cases, RPCLs may be processed by spinning from concentrated solution but usually this is possible only in very drastic conditions, because of the low solubility of these polymers. Also, in this case, the insertion of side groups may be effective in increasing solubility in organic solvents.[18,19] Other major problems are the "peeling" effect and the low resistance to compression.[20−24] These problems arise from the strong anisotropy of fibers, which exhibit high modulus along the fiber axis and a low one in the perpendicular direction. The reason can be attributed to weak chain-to-chain transversal interactions: the insertion of dipolar groups along the chain, as for example the polyamide, may reduce such an effect. Cross-linking acts in the same way, by increasing fiber transversal cohesion.[20−24]

In this paper, we report on the synthesis and characterization, including molecular structure refinement, of a new class of RLCPs with the following formula:

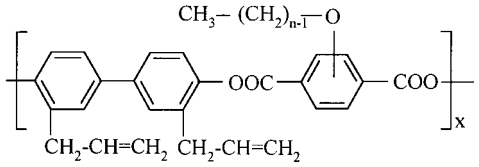

R(n) n=1-10

The effect of the lateral substituents on the thermal behavior and molecular packing in the solid state is discussed. The insertion of allyl groups onto aromatic rings in order to provide a reactive group suitable for chemical cross-linking has already been reported.[25−27] In this paper, we discuss thermal cross-linking and its effect on tensile properties of **R(5)** and **R(10)**.

Experimental Section

Polymer Synthesis. All reagents were used as obtained from Aldrich. **R(*n*)** were synthesized by interfacial polycondensation reaction of 3,3′-diallyl-4,4′-dihydroxybiphenyl (**1**) and the appropriate alkoxyterephthaloyl chloride (**2**). Compounds **1** and **2** were synthesized as outlined in refs 14 and 28, respectively. Approximately 1.5 g of **1** was dissolved in 100 cm^3 of water with 3% excess KOH and 0.700 g of benzyltriethylammonium chloride. The equimolar amount of the appropriate alkoxyterephthaloyl chloride was dissolved in 50 cm^3 of chloroform. The two solutions were stirred vigorously in a blender for 8 min. The polymer was precipitated by addition of *n*-heptane (100−150 cm^3) and, after filtration, washed three times with a chloroform/heptane (30/70 v/v) solution, once with 95% ethanol, and three times with water. Finally, the polymer was washed with 95% ethanol and dried at 60 °C under vacuum. Molecular weights evaluated by gel permeation chromatography (GPC) are given in Table 1.

* Corresponding author. E-mail: Iannelli@dica.unisa.it.
† Università di Napoli.
‡ Istituto per la Tecnologia dei Materiali Compositi-CNR.
§ Università di Salerno.

10.1021/ma000821o CCC: $19.00
Published on Web 11/18/2000

Table 1. Data Concerning Samples of R(*n*) (Melting Temperatures Measured at the Maximum of the Endothermic Transition)

polymer	^1T_d[d]	^2T_d[d]	T_s[e]	T_a[f]	T_m[g]	ΔH_m[h]	M_w ($\times 10^3$)
R(1)[a]	382	325	~180				154
R(2)[b]	383	332	~140				78
R(3)[b]	396	386[i]	~120		[189[j]]	[1.2[j]]	85
R(4)[c]	350	300		170	187	16.3	125
R(5)[c]	366	304		180	196	23.4	182
R(6)[c]	366	336		150	171	16.8	161
R(7)[c]	378	316		145	157	11.2	235
					[133[k]]	[0.29[k]]	
R(8)[c]	405[i]	404[i]		120	111−132	9.4	154
					[117[k]]	[0.11[k]]	
R(9)[c]	418[i]	398[i]		105	120	11.3	126
R(10)[c]	374	296		115	130	14.7	200

[a] Virgin powder sample. [b] Virgin fibrous sample. [c] Annealed fibrous sample (annealed for 3 h at T_a). [d] T_d/°C, temperature at which 5% of weight loss is observed in the TGA trace (^1T_d measured under nitrogen flow, ^2T_d measured in static air). [e] T_s/°C, softening temperature. [f] T_a/°C, annealing temperature. [g] T_m/°C, melting temperature. [h] ΔH_m/J g^{-1}, melting enthalpy. [i] Onset of a fast degradation phenomenon. [j] LC to LC transition observed in the DSC runs of virgin fiber samples of **R(3)** (see Figure 3). [k] Monotropic liquid-crystalline to nematic transition observed in the DSC runs of virgin fiber samples of **R(7)** and **R(8)** (see Figure 4).

The proton resonance data are in agreement with the expected values. For example, proton resonance data at 25 °C for **R(5)** [chloroform as solvent] are

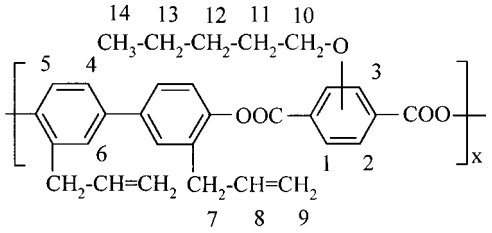

^{1}H NMR [δ (ppm), 1−2 (7.9, m); 3 (8.1, s); 4,5 (7.5, m); 6 (7.3, s); 7 (3.5, d); 8 (6.0, m); 9 (5.1, m); 10 (4.3, m); 11 (1.9, m); 12 (1.5, m); 13 (1.3, m); 14 (0.9, m)].

Characterization. Fibers were extruded from the nematic phase and cooled to room temperature. The average diameter of fibers is 200−300 μm.

Thermal measurements were carried out by means of a DSC-7 Perkin-Elmer calorimeter under nitrogen flow at a 10 °C/min rate.

Thermogravimetric analysis was performed by a Mettler TGA apparatus at 20 °C/min both under nitrogen flow and in static air.

Polarized optical microscopy was performed by means of a Jenapol microscope fitted with a Linkam THMS 600 hot stage.

Fiber diffraction spectra were recorded under vacuum by means of a cylindrical camera with a radius of 57.3 mm and the X-ray beam direction perpendicular to the fiber axis (Ni-filtered Cu−Kα radiation). The Fujifilm MS 2025 imaging plate and a Fuji Bioimaging analyzer System, model BAS-1800, were used for digitizing the diffraction patterns. High-temperature X-ray diffraction patterns were collected using a flat camera and a modified Linkam THMS 600 hot stage.

The ^{1}H NMR spectra were recorded in $CDCl_3$ solution with a Brucker DRX/400 spectrometer. Chemical shifts are reported relative to the residual solvent peak ($CHCl_3$: $\delta_H = 7.26$ ppm).

A Waters 150-C ALC/GPC instrument was used for GPC analysis, equipped with six 300 × 7.5 mm^2 columns (Waters Styragel HT3, HT4, HT5, HT6, 500 Å and 400 Å) and a Jasco 875 UV detector set at 254 nm (polystyrene as standard and chloroform as solvent, at 1 mL/min and 30 °C).

Dynamic mechanical tensile analysis was carried out by means of a Perkin-Elmer DMA 7 analyzer, in the temperature range between 20 and 300 °C at a 5 °C/min heating rate under nitrogen flow. Fiber length was approximately 15 mm and diameter was 300 μm. Frequency was set at 1 Hz, with dynamical load ranging from 10 to 210 mN.

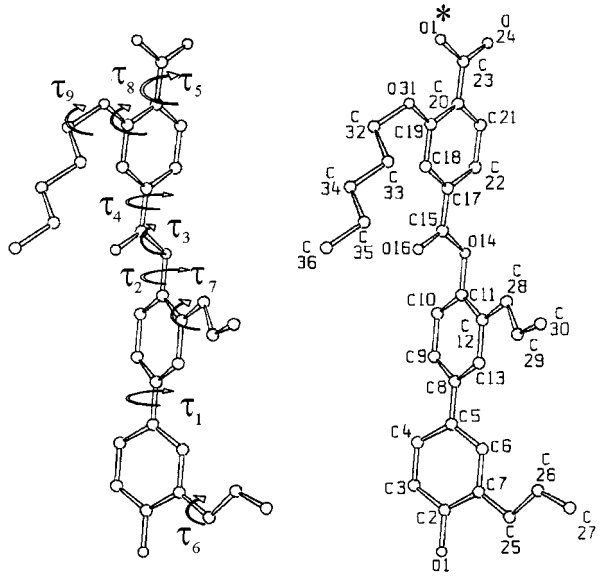

Figure 1. Asymmetric unit of the crystalline packing of **R-(5)**.

Structure Refinement Procedure. The "Whole Pattern" method[29] is used to carry out the analysis and the refinement of the crystalline structure. The method applies the least-squares fitting procedure to obtain the best match between the two-dimensional experimental and calculated X-ray diffraction patterns. Computation is carried out in the reciprocal space.

Parameters to be refined are of two kinds: (i) nonstructural ones, like the crystalline size and the degree of crystallites orientation with respect to the fiber axis, and (ii) structural ones, like the torsion angles defining chain conformation. The former affects the shape and the latter the diffraction intensity of each diffraction spot.

In this article, we have considered the following nonstructural parameters: (a) the averaged crystallite size [Δa, Δb, and Δc] taken along a direction parallel to the lattice axes [a, b, and c, respectively]; (b) the average angle [α_0] between the c lattice axis of crystallites and the fiber axis. α_0 is related to the degree of fiber orientation.

The structural parameters to be refined are as follows: (a) lattice parameters defining the unit cell; (b) fractional coordinates of the center of mass of the chain (x_0, y_0, z_0), and the angle of rotation (Φ_0) of the chain [Φ_0 is defined as the angle between two planes intersecting each other along a line connecting atoms O1 and O1* (see Figure 1). One plane is parallel to (010) while the second one contains atom C6]; (c) torsion angles τ_i defining chain conformation as shown in Figure 1.

The following structural parameters are fixed during refinement: (i) bond lengths C−C = 1.54 Å, aromatic C═C = 1.40 Å, double bond C═C = 1.45 Å, C═O = 1.23 Å, C−O = 1.43 Å, C−H = 1.08 Å, (ii) bond angles O−C−C = 109.5°, ester C−O−C = 120°, ether C−O−C = 109.5°, O−CO−C = 120°, C−C═C = 120°, aromatic C−C−C = 120°, and (iii) torsion angles τ_4 (O14−C15−C17−C18) = τ_5 (C21−C20−C23−O1*) = 180°, corresponding to the planar terephthaloyl unit. The isotropic thermal parameter $B_{iso} = 7.11$ Å^2, equal for all atoms, is not refined because of its strong correlation with the scale factor. Hydrogen atoms, located according to the canonical sp^2 and sp^3 geometry, are included in the calculation. During refinement, a constraint is imposed to the chain backbone in order to force the chain length to match the c axis length.

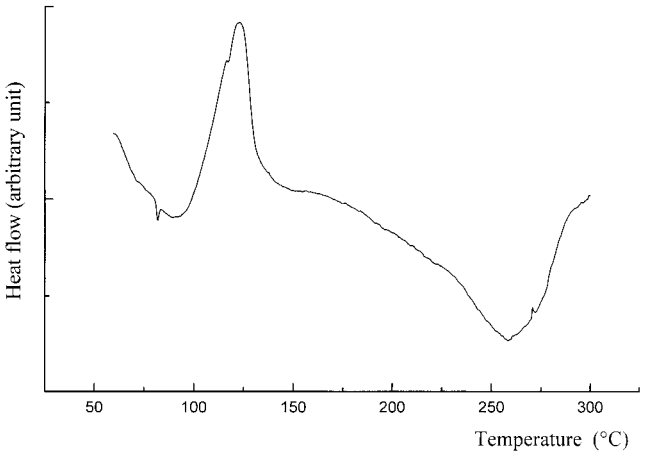

Figure 2. DSC first heating run of a powder sample of **R(8)**.

Discussion

Thermal Characterization. R(*n*) are soluble in chloroform at room temperature. Solubility increases with the length of side group of the terephthaloyl moiety.

According to the X-ray diffraction analysis (next section) and the optical microscopy (see below), the nematic phase is stable above melting or softening point for **R(*n*)** with $n > 3$. No definitive answer can be given for $n \leq 3$, because the phase behavior is disturbed by a fast cross-linking process that takes place after the softening temperature. Isotropization of **R(*n*)** is never observed, up to thermal decomposition starting at about 400−450 °C. This is in agreement with the rigid-rod character of polymers. Indeed we cannot exclude that the isotropization is hampered by the cross-linking reaction that occurs at high temperature even for $n > 3$. In fact, after a fast heating to 200 °C, polymers with $n > 3$ are still soluble in chloroform, but heating to a higher temperature induces the spontaneous cross-linking reaction, resulting in insoluble and swelling material. The cross-linking reaction is sometimes detectable as a broad exothermic peak in the DSC heating trace over 200 °C. For example, this peak is centered at about 260 °C in the case of **R(8)** (Figure 2). According to the TGA analysis, this phenomenon does not correspond to the degradation of material, in fact the weight loss starts at about 350 °C (Table 1). TGA runs of **R(*n*)** taken under nitrogen flow show a single-step degradation process. In static air, degradation starts at lower temperature, as expected, and it is characterized by a two-step process. The first one probably corresponds to the side group oxidation, the aliphatic moiety being more prone to oxidation than the aromatic moiety. Moreover, the TGA trace in static air shows a slight increase of weight (approximately 2.5 wt %) in the range 220−280 °C, corresponding to oxygen addition to the double bond of allyl groups.

R(*n*) can be classified into three groups:

(a) $1 \leq n \leq 3$. No clear melting peak is observed in the DSC heating run. For **R(1)** two broad step transitions are evident at 130 °C and 172 °C (Figure 3). Optical microscopy analysis show a solid to a fluid LC phase transition in the range 120−180 °C according to Table 1, followed by a very fast cross-linking that freeze the anisotropic fluid. **R(2)** and **R(3)** can be extruded with some difficulty to form highly oriented fibers. Moreover, **R(3)** shows a reversible endothermic peak at 189 °C, which may be attributed to a LC to LC transition, according to the small undercooling (Figure 3) and the small transition enthalpy (Tables I). No optical texture characteristic of a specific LC phase was observed;

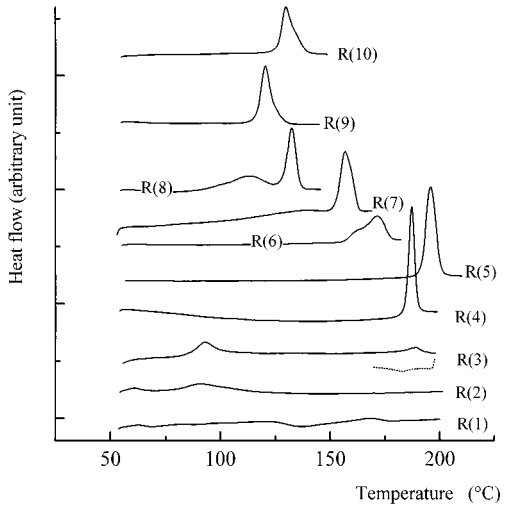

Figure 3. DSC first heating run of **R(*n*)**. Analysis is performed on virgin powder sample of **R(1)**, virgin fiber sample of **R(2)** and **R(3)**, and annealed fiber sample of **R(4)**−**R(10)** according to Table 1.

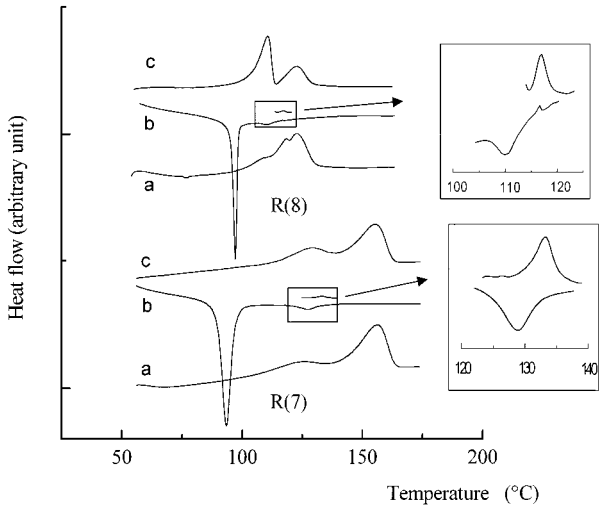

Figure 4. DSC of **R(7)** and **R(8)**: (a) first heating, (b) first cooling, and (c) second heating run. The monotropic LC-to-nematic transition is shown on an enlarged scale in the inset (this transition was isolated by a fast heating after the nematic-to-LC transition in the cooling run).

(b) $4 \leq n \leq 7$. Virgin powder samples show a mesophasic structure at room temperature and crystallize upon annealing. Fibers exhibit the same behavior of virgin powder samples. The crystalline phase, obtained by annealing, is very well developed resulting into sharp and intense spots in the X-ray diffraction pattern (see next section). **R(7)** shows a different diffraction pattern with respect to the other members of the group and, as well as **R(8)** of next group, a small reversible endothermic transition in the heating run (Figure 4) which may be ascribed to a monotropic LC to nematic phase transition. The exact nature of this liquid crystalline phase could not be established by X-ray diffraction analysis because crystallization takes place during measurement. Even in this case no optical texture characteristic of a specific LC phase was observed;

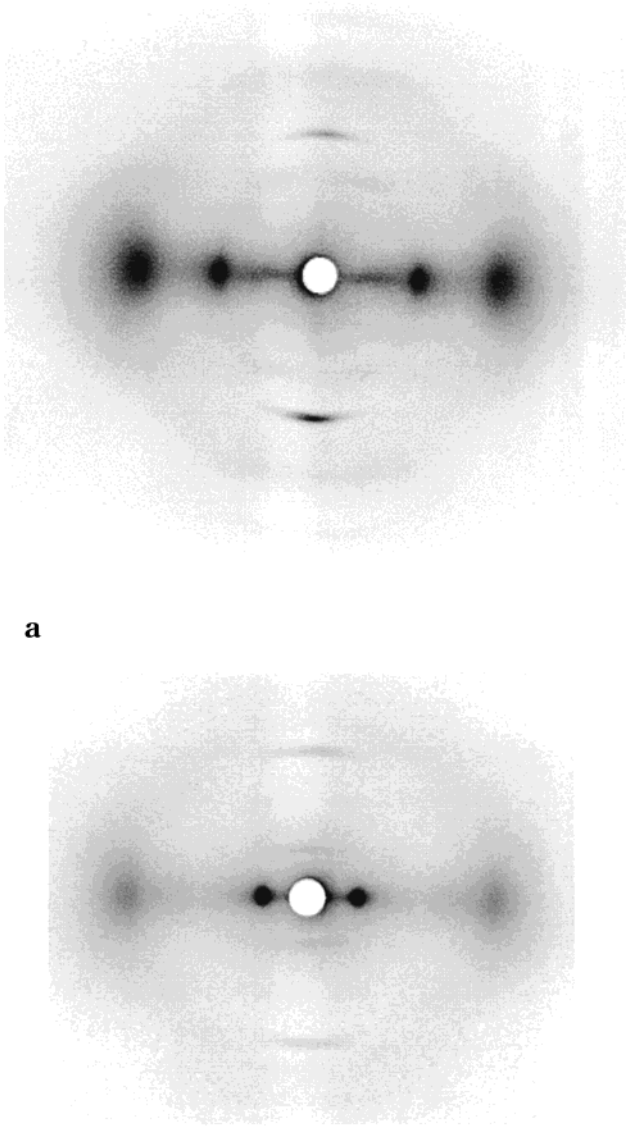

Figure 5. X-ray diffraction pattern of a virgin fiber sample of **R(2)** (a) and **R(10)** (b). Measurement was taken at room temperature **(**fiber axis vertical).

(c) $8 \leq n \leq 10$. Virgin powder samples as well as fibers show only the mesophase, no crystallization being induced by annealing. Melting temperature is lower than that of previous group (110−130 °C).

Preliminary X-ray Diffraction Analysis. Virgin powder samples of **R(*n*)**, with the exception of **R(1)**, show a mesophasic structure stable at room temperature which is retained in fibrous samples. In particular, X-ray diffraction pattern of fibers are characterized by a strong reflection at low angles, whose position depends on the length of the aliphatic side group (Figure 5). The corresponding spacing increases linearly when plotted vs *n* (see Figure 6). **R(2)** scatters from this trend, with a spacing shorter than the expected one. This might be ascribed to a modification of the molecular packing, which contains a single chain per unit cell in the case of **R(2)**, while a two-chain unit cell is observed for the other polymers (see next section). In the average, the spacing increases by 2 Å per two methylene units of the side alkoxy group, despite the value of 2.54 Å calculated for a full extended trans-planar conformation. The

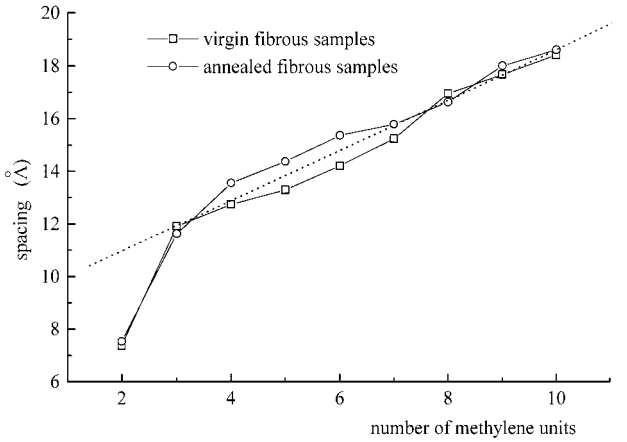

Figure 6. Spacing corresponding to the low angles reflection plotted vs the number of methylene units of the side alkoxy group of **R(*n*)**.

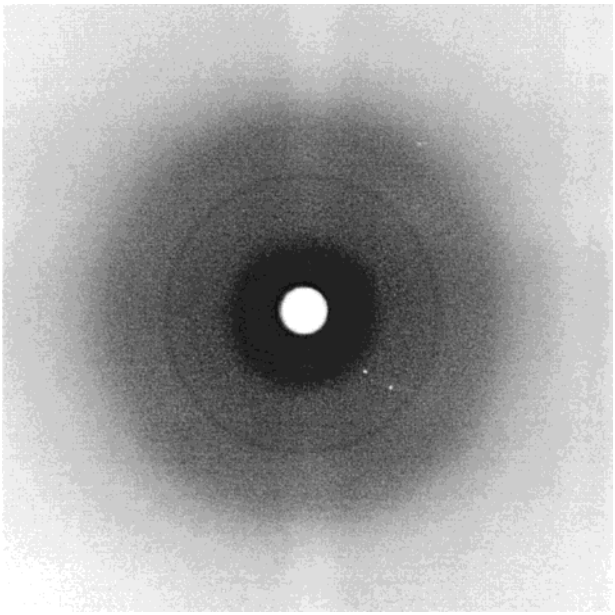

Figure 7. X-ray diffraction pattern of virgin powder sample of **R(1)**.

reason may be a deformation of the most extended conformation as well as a slight tilt of alkoxy group with respect to the lattice vector corresponding to the reflection at low angles. The repeating unit length along chain direction is about 16.9 Å, calculated from layer lines in the diffraction patterns of both virgin and annealed fibers. This value corresponds to the most extended chain conformation as expected for rodlike polymers.

In some cases, the molecular structure of fibrous samples undergoes rearrangement upon annealing, resulting in the following modification of diffraction pattern:

(i) **R(1)** has an "amorphous-like" behavior, probably due to spontaneous cross-linking that prevents crystallization process, as already discussed. In fact, the X-ray diffraction pattern of **R(1)** recorded at different temperatures do not shown any diffraction spot, except for a weak and sharp reflection with a spacing of 5.50 Å (Figure 7). This spacing corresponds to a Bragg meridional reflection that is always present in the diffraction pattern of **R(*n*)**. This suggests that a repeating moiety along a direction almost parallel to the chain axis is always present and that it is almost equal to one-third

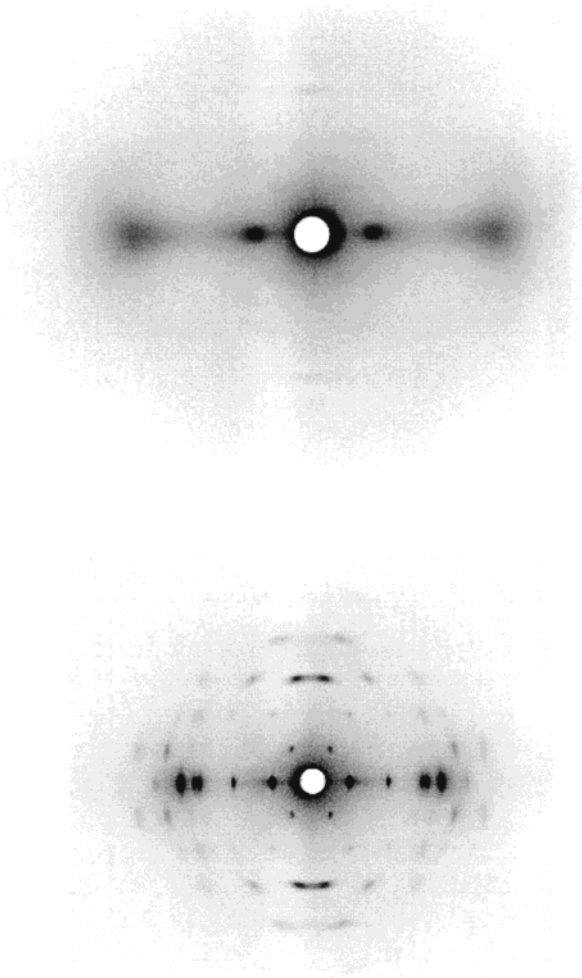

Figure 8. X-ray diffraction patterns of fiber sample of **R(5)**: (a) virgin sample; (b) sample annealed for 3 h at 180 °C (fiber axis vertical). Measurement was taken at room temperature.

of the monomeric unit length. This periodicity corresponds to the reflection with Bragg indices $\bar{2}03$ in the case of the crystalline phase of **R(5)** (see next section). In the case of **R(2)** and **R(3)** this reflection is the strongest one in the meridian. **R(2)** and **R(3)** fibers are not affected by annealing to any extent.

(ii) Crystallization is induced even by a short annealing (a few minutes) in the case of **R(4)**, **R(5)**, and **R(6)**. The diffraction pattern of crystalline fibers shows very sharp and polarized spots (Figure 8).

(iii) **R(7)** fiber crystallizes similarly to previous polymers. The resulting diffraction pattern shows more reflections at low angles (Figure 9), indicating that unit cell is bigger. Even so, strong similarity between the X-ray diffraction patterns of **R(7)** and those of **R(4)**, **R(5)** and **R(6)** still remains;

(iv) Finally, **R(*n*)** fibers with $7 < n \leq 10$ are not affected by annealing similar to **R(2)** and **R(3),** and the only phase observed at room temperature is the mesophase.

Previous remarks suggest that increasing flexible side group length (thus increasing folding and molecular mobility of side group) destabilizes the crystalline ordered phase, which is not observed any longer for $n > 7$. No definitive answer can be given for **R(1)**, **R(2),** and **R(3)** because their high reactivity might hamper the crystallization by quenching the mesophasic structure.

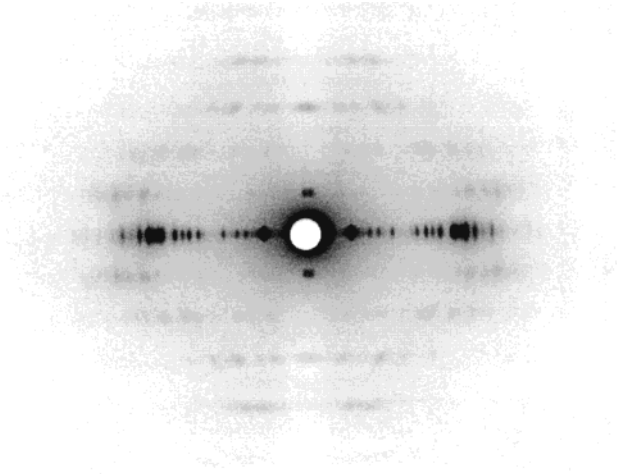

Figure 9. X-ray diffraction pattern of an annealed fiber sample of **R(7)** (3 h at 145°; fiber axis vertical). Measurement was taken at room temperature.

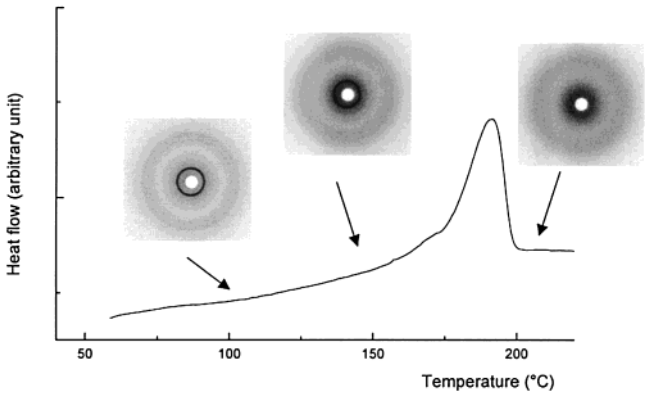

Figure 10. DSC first heating run of powder sample of **R(5)** showing the X-ray diffraction pattern at different temperatures.

According to the X-ray diffraction analysis, the nematic phase is stable after melting for polymers with $n > 3$. For instance, reflections at high angles become broader and less intense during heating in the diffraction pattern of **R(5)** (Figure 10), but the strong low-angle reflection is still present before melting. All reflections disappear after melting at 195 °C, and only a diffuse halo compatible with the nematic phase is visible [halo peaked at $(\sin\theta)/\lambda = 0.11$ Å^{-1} and no Bragg diffraction for lattice distances lower than about 41 Å].

In a previous investigation, we have reported the synthesis and the characterization of a class of nematic rigid-rod polymers with the formula[16]

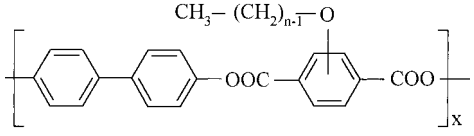

R'(n) n=1,3,5,7

R′(*n*) are analogous to **R(*n*)** with no allyl units attached to the biphenyl unit. Only **R′(1)** can be crystallized by annealing while a mesophase, similar to that of **R(*n*)**, is observed for longer side groups. In this case,

Table 2. Cell Parameters[a]

polymer	*a*	*b*	*c*	*β*
R(4)	15.71(1)	5.53(1)	17.0(1)	120.4(1)
R(5)	16.93(1)	5.03(1)	16.98(1)	119.8(1)
R(6)	17.70(1)	5.27(1)	16.98(1)	118.9(1)

[a] Cell parameters obtained by the least-squares fitting of the 10 most strong spots in the diffraction pattern.

annealing does not affect molecular packing. The temperature of solid to nematic phase transition (about 280 °C, independent of *n*) is higher than that of **R(*n*)**, as expected for the absence of the two allyl groups.

R(4)−R(6) Molecular Structure Determination. Lattice parameters have been evaluated by least-squares refinement using at least 10 of the strongest Bragg reflections in the diffraction pattern. They are reported in Table 2. The monoclinic cell, space group $P2_1$, unique axis *b* (two chains per unit cell), was assumed on the basis of the extinct reflections in the experimental diffraction pattern. **R(5)** was chosen as the representative term of the group, the crystalline phase of these polymers being the same.

Starting from the lattice parameters given in Table 2, in the first stage of the structure analysis of **R(5)** torsion angles were set to $\tau_1 = 0°$, $\tau_2 = 180°$, $\tau_3 = 180°$, $\tau_6 = \tau_7 = 180°$, $\tau_8 = 60°$, and $\tau_9 = 180°$. The chain center of mass was placed at $x_0 = 0.20$ and $z_0 = 0.25$, both to avoid steric interactions and to ensure strong 100 and 210 reflections, according to the equatorial observed data. Because of the statistical insertion of the terephthaloyl moiety along the chain (*up* and *down* statistic), two side groups should be considered, each taken into account during structural analysis with an occupancy factor of 0.5. To reduce the number of parameters to be refined, the two aliphatic groups were taken one the mirror image of the other with respect to a mirror plane placed perpendicular to the terephthaloyl unit. For the same reason, in the first stage of the analysis a mirror plane is imposed to the biphenyl unit passing through the middle of phenyl-to-phenyl bond ($\tau_1 = 0°$). The latter constraint was removed at the final stage of the refinement. Concerning the lateral groups, only torsion angles τ_8 and τ_9 of the alkoxy unit and torsion angle τ_6 of allyl group (with constraint $\tau_7 = 360° - \tau_6$) were refined because any attempt to consider more torsion angles failed. In fact, a large fluctuation takes place, and no convergence of the least-squares procedure can be reached.

Following the procedure described in previous articles [29−32] and briefly summarized in the Experimental Section, the convergence of refinement is reached in few steps and the experimental diffraction pattern is well reproduced.

The observed and the calculated diffraction data at the end of the refinement are compared in Figure 11. A representation of the crystalline packing is shown in Figures 12 and 13. The refined atomic fractional coordinates and the refined parameters are listed in Tables 3 and 4, respectively. All the intra- and intermolecular atomic distances are in agreement with the standard values excepted for the intermolecular short contact between adjacent biphenyl units (2.86 Å for C9−C14 and 2.94 Å for C11−C12) and between side groups. Indeed, the statistical character of the structural model, which is employed to account for *up* and *down* insertion of the alkoxyterephthaloyl unit along the chain (*tail-to-tail* or *tail-to-head* sequence of monomers), should be kept in mind. Consequently, the refined structure is not a "true one" but only the average of several structures, each being stereochemically consistent.

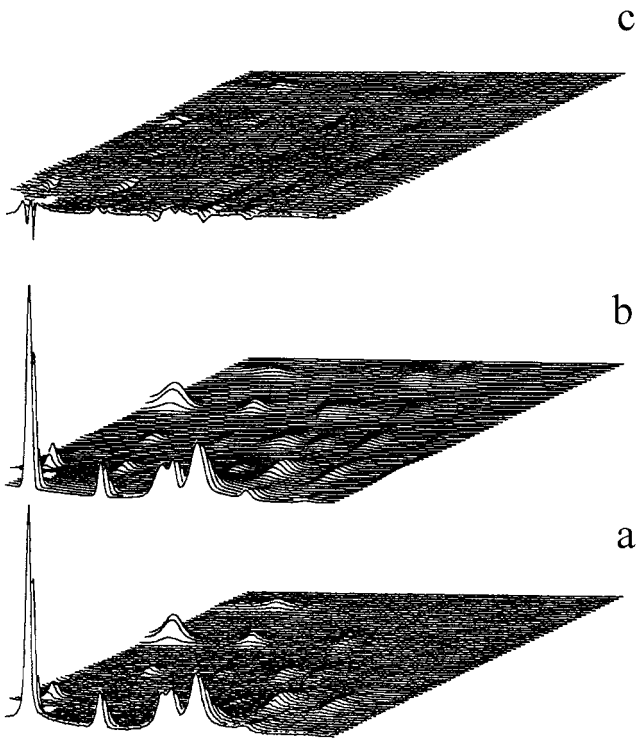

Figure 11. Three-dimensional representation of X-ray diffraction pattern of **R(5)** (crystalline phase): (a) observed data; (b) calculated data; (c) the difference between parts a and b.

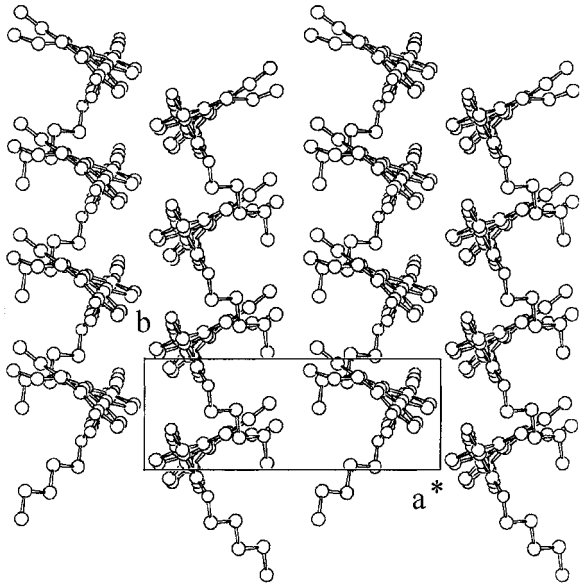

Figure 12. Molecular packing of **R(5)** (crystalline phase) viewed along the *c* axis.

The molecular packing is characterized by a layered organization of chains promoted by the ester-to-ester dipole interactions, in a way that has been already reported for similar polymers.[6,13,19] This organization is the result of the "incompatibility" between the rigid chains and the flexible side groups. This may explain why crystalline phase is disrupted by a side alkoxy group longer than the heptyloxy unit: an ordered molecular arrangement of the alkoxy unit with the short allyl groups is no longer possible.

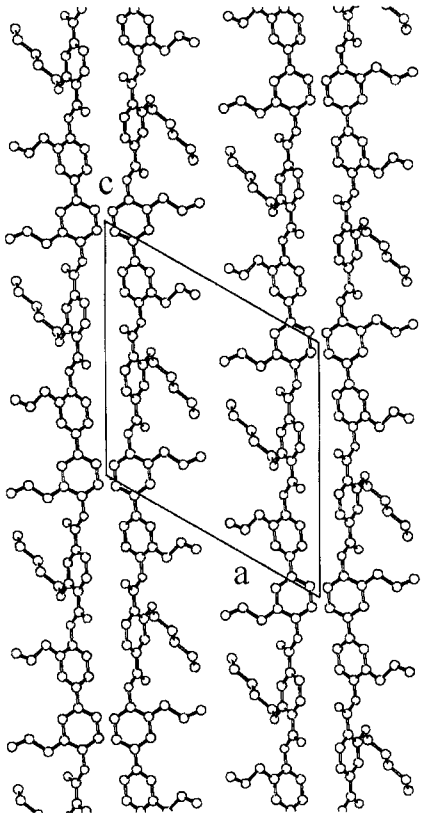

Figure 13. Molecular packing of **R(5)** (crystalline phase) viewed along the *b* axis.

Table 3. R(5) Atomic Fractional Coordinates after Refinement (Standard Deviation in Parentheses)

atom	*x*	*y*	*z*
O1	0.1674(3)	0.0000(0)	−0.3242(3)
C2	0.1584(7)	0.0289(2)	−0.2490(8)
C3	0.092(5)	−0.1098(9)	−0.240(1)
C4	0.083(6)	−0.080(1)	−0.162(2)
C5	0.140(2)	0.0885(6)	−0.094(2)
C6	0.207(3)	0.227(1)	−0.104(2)
C7	0.216(3)	0.1971(9)	−0.181(1)
C8	0.131(3)	0.1183(8)	−0.017(3)
C9	0.047(8)	0.059(2)	−0.021(3)
C10	0.037(9)	0.089(2)	0.056(4)
C11	0.113(4)	0.178(1)	0.138(5)
C12	0.197(2)	0.237(1)	0.141(4)
C13	0.206(3)	0.207(1)	0.064(4)
O14	0.104(4)	0.207(1)	0.213(6)
C15	0.144(2)	0.0280(9)	0.285(6)
O16	0.182(1)	−0.160(1)	0.277(6)
C17	0.1400(2)	0.0657(7)	0.364(7)
C18	0.179(1)	−0.1093(8)	0.435(7)
C19	0.1749(7)	−0.0716(6)	0.515(8)
C20	0.131(3)	0.1411(8)	0.524(9)
C21	0.092(5)	0.316(2)	0.453(8)
C22	0.096(5)	0.278(2)	0.374(7)
C23	0.127(3)	0.1788(9)	0.604(9)
O24	0.088(5)	0.367(2)	0.612(9)
C25	0.282(8)	0.336(2)	−0.190(1)
C26	0.350(12)	0.458(4)	−0.098(1)
C27	0.420(17)	0.600(5)	−0.091(1)
C28	0.272(7)	0.326(2)	0.223(5)
C29	0.361(13)	0.318(5)	0.216(4)
C30	0.442(19)	0.395(6)	0.286(5)
O31	0.213(3)	−0.242(1)	0.583(9)
C32	0.224(4)	−0.474(2)	0.548(8)
C33	0.307(9)	−0.458(4)	0.532(8)
C34	0.319(11)	−0.708(4)	0.494(7)
C35	0.402(16)	−0.693(6)	0.478(7)
C36	0.413(17)	−0.943(7)	0.440(6)

Thermal Cross-Linking and Tensile Analysis. In previous investigations we found that liquid crystalline polymers (LCPs) bearing allyl units as pendant groups can cross-link under suitable conditions.[25−27] Allyls are quite stable to mild thermal treatment up to 200 °C; thus, in some cases, thermal processing of polymers is possible before cross-linking takes place. This is also the case for **R(*n*)**. Cross-linking of such LCPs can be promoted in different ways. Thermally cross-linking activated by peroxides is successful when activator can be incorporated in the sample: this is the case of both films prepared by casting from solvent containing the activator, or solid samples dipped into activator solution. In the latter case samples should be not soluble. The exposure of samples to UV or γ radiation is more attractive, due to a faster and easier procedure. In this case, samples can be cross-linked freezing their morphology and macroscopic shape at room temperature.[26,27] Because the cross-linking reaction occurs in the solid state, one has the attractive opportunity of quenching ordered molecular architectures. We assumed that solid state cross-linking is allowed by the short distance between allyl units in the solid state molecular packing. In fact, due to their "incompatibility", chains and pendant groups spontaneously "segregate" each other, giving rise to a lamellar (layered) or bundle molecular organization with a short allyl-to-allyl distance. This was reported to be the case of polymers **P′(5)**[25] and **P(12)**,[27] with lamellar structure, and **PA(10)**,[26] with a bundle structure. Their formula are, respectively

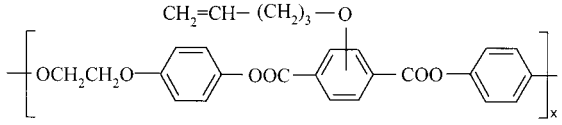

P′(5)

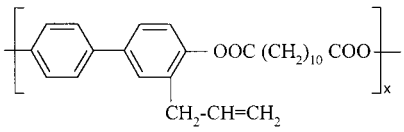

P(12)

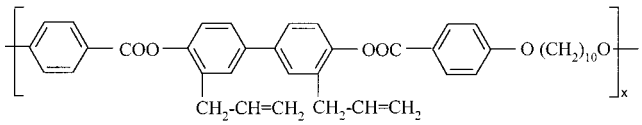

PA(10)

All these polymers cross-link in the solid state. In previous sections, we have shown that the crystalline phase observed for **R(*n*)** with $n = 4-6$ is of the lamellar type. Similar to **P(5)′** and **P(12)**, allyl units are packed close to each other; thus, the requirement of an adequate short distance between allyl units to promote cross-linking in the solid state is fulfilled. The crystalline phase is not observed for **R(*n*)** with $n > 7$, as previously discussed, probably because the increased difference in length between the allyl and aliphatic units adversely affects the packing of pendant groups. Even so, the lamellar organization is preserved according to the spot at low angles in the diffraction patters of polymers. It follows that, even in the mesophase of **R(*n*)** with $n > 7$, allyl units are tightly packed, but in a less ordered fashion.

To freeze the macro-orientation of fibrous samples of **R(*n*)**, the use of peroxide thermal activation is not

Table 4. R(5) Parameters at the End of the Structural Refinement

Structural Parameters			
$a = 16.55(2)$ Å	$b = 5.373(5)$ Å	$c = 16.92(2)$ Å	$\beta = 119.9(1)°$
$x_0 = 0.1674(3)$	$y_0 = 0$	$z_0 = -0.3242(3)$	$\Phi_0 = 65.3(2)°$
$\tau_1 = 23.9(2)°$ (C4−C5−C8−C9)	$\tau_2 = 257.2(2)°$ (C10−C11−O14−C15)	$\tau_3 = 183.9(2)°$ (C11−O14−C15−C17)	$\tau_6 = 166.9(7)°$ (C2−C7−C25−C26)
$\tau_7 = 193.2(7)°$ [a] (C11−C12−C28−C29)	$\tau_8 = 19.9(2)°$ (C18−C19−O31−C32)	$\tau_9 = 284.5(3)°$ (C19−O31−C32−C33)	
Nonstructural Parameters			
$\Delta a = 161.0(3)$ Å	$\Delta b = 57.9(2)$ Å	$\Delta c = 89.6(2)$ Å	$\alpha_0 = 5.09(1)$

[a] Constrained condition: $\tau_7 = 360° - \tau_6$.

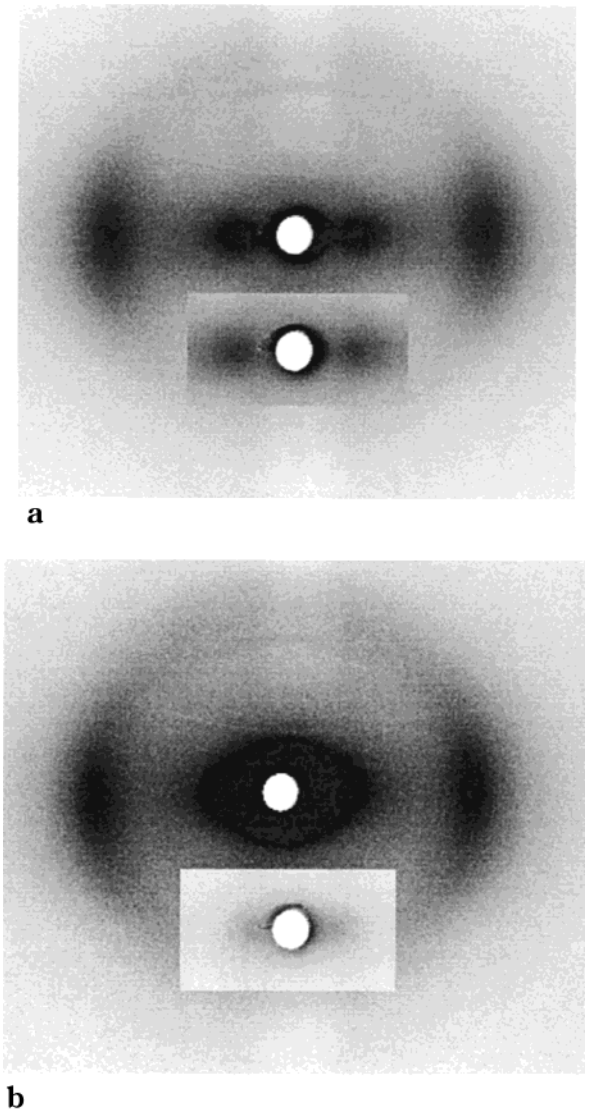

Figure 14. X-ray diffraction pattern of cross-linked fiber sample of **R(5)** (a) and **R(10)** (b) [fiber axis vertical]. Fibers were reannealed for 3 h at 180 and 115 °C, respectively. The low-angle area is also shown with a lower contrast.

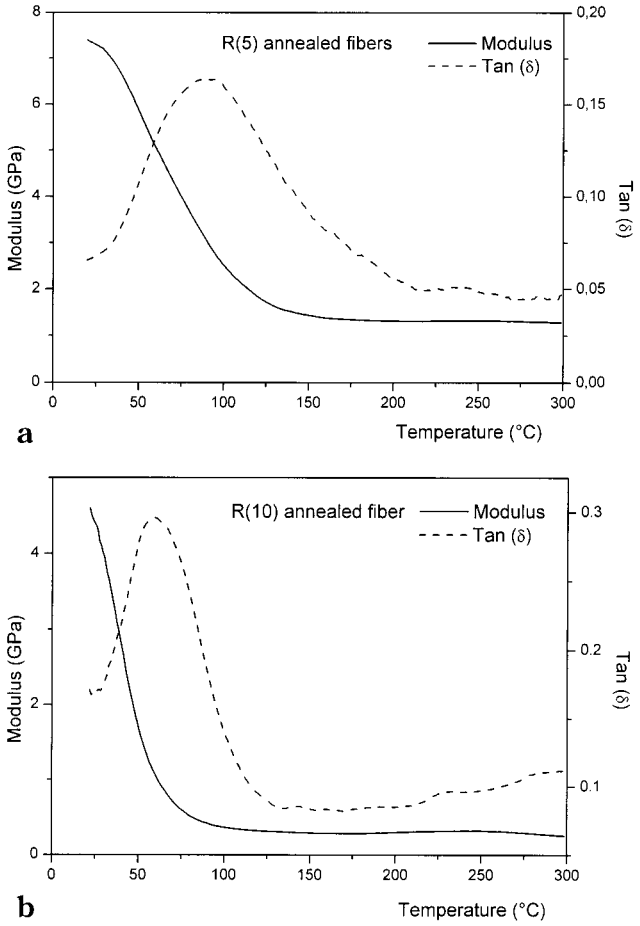

Figure 15. Dynamic tensile measurements: modulus and tan(δ) are drawn for cross-linked fibers of **R(5)** (a) and **R(10)** (b).

possible because of the fast cross-linking reaction that occurs during thermal processing of fibers. Moreover, samples of **R(*n*)** cannot be dipped in solution of the activator to be absorbed because of the good solubility of polymers. Nevertheless, we observed that an appropriate annealing in the solid-state promote the spontaneous cross-linking of polymers without the use of any activator. The process is quite slow for **R(*n*)** with $n > 3$, as we already stated, but annealing for approximately 60 min was found to be adequate to freeze fiber morphology. As a preliminary test, we decided to perform 3 h of annealing at a temperature approximately 15 °C lower than the melting temperature for two polymers of the series: **R(5)** exhibiting the crystalline phase and **R(10)** exhibiting the mesophase. Fibers of these two polymers were annealed under vacuum respectively at 180 and 115 °C, followed by a further annealing of 10 min at 300 °C to increase the degree of cross-linking. During thermal treatment fibers of **R(10)** shrank, and at the end of the process, they become quite distorted in shape, while fibers of **R(5)** were completely unaffected. We repeated the whole procedure on virgin fibers of **R(10)** fixing their tips with a little spring. At the end of thermal treatment all fibers are insoluble in boiling chloroform and their DSC traces do not show any melting peak. The X-ray diffraction patterns of fibers show that the orientation is preserved and that the phase stabilized by the whole treatment is the mesophase for **R(5)** (Figure 14a), while the lamellar structure is disrupted for **R(10)** (Figure 14b). Further

annealing at 180 °C does not promote structural reorganization, showing that cross-linking limits molecular mobility.

Tensile measurements taken according to the Experimental Section are reported in Figure 15. Both tensile modulus and tan(δ) vs temperature are shown. The trend is similar for both polymers, **R(5)** and **R(10)**, the major difference being the glass transition temperature, associated with the maximum in tan(δ) curve. Glass transition temperature is lower for **R(10)** (60 °C) with respect to **R(5)** (90 °C) because of the higher mobility of the longer pendant group. Tensile modulus decreases with increasing temperature until a constant value of approximately 1 GPa for **R(5)** and 0.5 GPa for **R(10)** is reached up to 300 °C. It is worth noting that virgin fibers, without any annealing treatment, melt under the conditions of tensile measurements.

The characterization of the actual cross-linking scheme and the evaluation of the cross-linking density are beyond the scope of the present work. In the case of **P(12)** we performed IR analysis of film samples cross-linked by UV irradiation or thermal activated reaction.[27] We observed that for this polymer approximately 50% of allyl units react and that a further prolonged treatment does not improve the conversion anymore. In the case of fibers, we could not perform IR analysis, but like film samples, we assumed that conversion of allyl units is not complete. We believe that even for **R(*n*)** allyls do not react completely.

Conclusion

We have shown that the rodlike polymers **R(*n*)** bearing side flexible groups can be synthesized by interfacial polycondensation at room temperature, exploiting the good solubility in chloroform. **R(*n*)** can be processed and cross-linked by annealing at adequate temperature. Only polymers with $n < 3$ undergo a fast cross-linking, thus complicating material processing. In particularly, **R(1)** gives rise to an anisotropic and not crystalline network when heated to 180 °C.

A crystalline phase with a layered molecular packing is observed for **R(4)**, **R(5)**, and **R(6)**. This phase is characterized by chain-to-chain contact and side groups segregation similarly to that reported for analogous polymers. Longer side group destabilizes the crystalline phase which is not observed for $10 \geq n > 7$. Indeed, for $n \leq 3$, no ultimate conclusion can be drawn because spontaneous cross-linking might interfere with the crystallization process.

The layered structure promotes thermal cross-linking in the solid state because of the short distance between adjacent allyl groups. We found that annealing for 3 h at a temperature 15 °C lower than the melting temperature promotes cross-linking of fiber samples of **R(5)** and **R(10)**. Tensile analysis and X-ray diffraction show that cross-linking quenches the macro-orientation of samples.

We could not drawn any conclusion on the nature of cross-linkage obtained and on the degree of cross-linking reached, which are very important in order to fully characterize this class of RLCPs and other similar cross-linkable polymers. For this reason, further investigation is under scrutiny.

Acknowledgment. Support by Ministero dell'Università e della Ricerca Scientifica e Tecnologica in partially financing this research project is acknowledged (Progetto Nazionale: Sistemi Polimerici per Materiali Compositi).

References and Notes

(1) Yang, H. H. *Aromatic High-Strength Fibers*; SPE Monograph Series; Wiley Interscience: New York, 1989.
(2) Economy, J; Goranov, K. In *High Performance Polymers*, Advances in Polymer Science, Springer Verlag: Berlin, 1994, Vol. 117, p 221.
(3) Ballauff, M.; Schmidt, G. M. *Makromol. Chem., Rapid Commun.* **1987**, *8*, 93.
(4) Rodriguez-Parada; J. M.; Duran, R.; Wegner, G. *Macromolecules* 1**989**, *22*, 2507.
(5) Kricheldorf, H. R.; Engelhardt, J. *Macromol. Chem.* **1990**, *191*, 2017.
(6) Stern, R.; Ballauff, M.; Lieser, G.; Wegner, G. *Polymer* **1991**, *32*, 2017.
(7) Lee, K. S.; Kim, H. M.; Rhee, J. M.; Lee, S. M. *Macromol. Chem.* **1991**, *192*, 1033.
(8) Harkness, B. R.; Watanabe, J. *Macromolecules* **1991**, *24*, 6759.
(9) Watanabe, J.; Harkness, B. R.; Sone, M. *Polym. J.* **1992**, *24*, 1119.
(10) Bao, Z.; Chen, Y.; Coi, R.; Yu, L. *Macromolecules* **1991**, *26*, 5281.
(11) Centore, R.; Roviello, A.; Sirigu, A.; Kricheldorf, H. R. *Macromol. Chem. Phys.* **1994**, *195*, 3009.
(12) McCreight, K. W.; Ge, J. J.; Guo, M.; Mann, I.; Li, F.; Shen, Z.; Jin, X.; Harris, F. W.; Cheng, Z. D. *J. Polym. Sci., Phys. Ed.* **1999**, *37*, 1633.
(13) Iannelli, P.; Pragliola, S.; Roviello, A.; Sirigu, A. *Macromolecules* **1997**, *30*, 4247.
(14) Caruso, U.; Iannelli, P.; Roviello, A.; Sirigu, A. *J. Polym. Sci., Phys. Ed.* **1998**, *36*, 2371.
(15) Acierno. D.; Di Maio, L.; Iannelli, P. *J. Polym. Sci., Phys. Ed.* **1999**, *37*, 1601.
(16) Iannelli, P.; Caruso., U.; Pragliola, S.; Roviello, A.; Sirigu, A. *J. Polym. Sci., Chem. Ed.* **1998**, *36*, 263.
(17) Acierno, D.; Fresa, R.; Iannelli, P.; Vacca, P. *Polymer* **2000**, *41*, 4179.
(18) Galda, P.; Kistner, D.; Martin, A.; Ballauff, M. *Macromolecules* **1993**, *26*, 1595.
(19) Kricheldorf, H. R.; Domschke, A. *Macromolecules* **1994**, *27*, 1509.
(20) Jenkins, S.; Jacob, K. I.; Kumar, S. *J. Polym. Sci., Phys. Ed.* **1998**, *36*, 3057.
(21) Dang, T. D.; Wang, C. S.; Click, W. E.; Chuah, H. H.; Tsai, T. T.; Husband, D. M.; Arnold, F. E. *Polymer* **1997**, *38*, 621.
(22) Mehta, V. R.; Kumar, S.; Polk, M. B.; Vanderhart, D. L.; Arnold, F. E.; Dang, T. D. *J. Polym. Sci., Phys. Ed.* **1996**, *34*, 1881.
(23) Kumar, S.; Heiminiak, T. E. *The Materials Science and Engineering of Rigid-Rod Polymers*; Material Research Society Symposium Proceeding 134, Material Research Society: Pittsburgh, PA, 1989; p 363.
(24) Dotrong, M.; Dotrong, M. H.; Song, H. H.; Santhosh, U.; Lee C. Y−C.; Evers, R. C. *Polymer* **1998**, *39*, 5799.
(25) Di Maio, L.; Iannelli, P.; Pragliola, S.; Roviello, A.; Sirigu, A. *J. Polym. Sci., Phys. Ed.* **1998**, *36*, 433.
(26) Acierno, D.; Di Maio, L.; Iannelli, P.; Spadaro, G.; Valenza, A. *Polymer* **2000**, *41*, 6647.
(27) Acierno, D.; Fresa, R.; Iannelli, P.; Vacca, P. *Polymer* **2000**, *41*, 7785.
(28) Caruso, U.; Pragliola, S.; Roviello, A.; Sirigu, A.; Iannelli, P. *Macromolecules* **1995**, *28*, 6089.
(29) Iannelli, P. *J. Appl. Crystallogr.* **1994**, *27*, 1055.
(30) Iannelli, P.; Damman, P.; Dosière, M.; Moulin, J. F. *Macromolecules* **1999**, *32*, 2293.
(31) Iannelli, P. *Macromolecules* **1993**, *26*, 2303.
(32) Iannelli, P. *Macromolecules* **1993**, *26*, 2309.

MA000821O